



HAL
open science

Estimation of the caesium-137 source term from the Fukushima Daiichi nuclear power plant using a consistent joint assimilation of air concentration and deposition observations

Victor Winiarek, Marc Bocquet, Nora Duhanyan, Yelva Roustan, Olivier Saunier, Anne Mathieu

► To cite this version:

Victor Winiarek, Marc Bocquet, Nora Duhanyan, Yelva Roustan, Olivier Saunier, et al.. Estimation of the caesium-137 source term from the Fukushima Daiichi nuclear power plant using a consistent joint assimilation of air concentration and deposition observations. *Atmospheric environment*, 2014, 82, pp.268-279. 10.1016/j.atmosenv.2013.10.017 . hal-00907484v1

HAL Id: hal-00907484

<https://inria.hal.science/hal-00907484v1>

Submitted on 21 Nov 2013 (v1), last revised 26 Nov 2013 (v2)

HAL is a multi-disciplinary open access archive for the deposit and dissemination of scientific research documents, whether they are published or not. The documents may come from teaching and research institutions in France or abroad, or from public or private research centers.

L'archive ouverte pluridisciplinaire **HAL**, est destinée au dépôt et à la diffusion de documents scientifiques de niveau recherche, publiés ou non, émanant des établissements d'enseignement et de recherche français ou étrangers, des laboratoires publics ou privés.

Estimation of the caesium-137 source term from the Fukushima Daiichi nuclear power plant using a consistent joint assimilation of air concentration and deposition observations

Victor Winiarek^{a,b}, Marc Bocquet^{a,b}, Nora Duhanyan^a, Yelva Roustan^a, Olivier Saunier^c, Anne Mathieu^c

^a Université Paris-Est, CERE, joint laboratory École des Ponts ParisTech and EDF R&D, Champs-sur-Marne, France

^b INRIA, Paris Rocquencourt research centre, France

^c Institut de Radioprotection et de Sûreté Nucléaire (IRSN), PRP-CRI, SESUC, BMTA, Fontenay-aux-Roses, 92262, France

Abstract

Inverse modelling techniques can be used to estimate the amount of radionuclides and the temporal profile of the source term released in the atmosphere during the accident of the Fukushima Daiichi nuclear power plant in March 2011. In Winiarek et al. (2012b), the lower bounds of the caesium-137 and iodine-131 source terms were estimated with such techniques, using activity concentration measurements. The importance of an objective assessment of prior errors (the observation errors and the background errors) was emphasised for a reliable inversion. In such critical context where the meteorological conditions can make the source term partly unobservable and where only a few observations are available, such prior estimation techniques are mandatory, the retrieved source term being very sensitive to this estimation.

We propose to extend the use of these techniques to the estimation of prior errors when assimilating observations from several data sets. The aim is to compute an estimate of the caesium-137 source term jointly using all available data about this radionuclide, such as activity concentrations in the air, but also daily fallout measurements and total cumulated fallout measurements. It is crucial to properly and simultaneously estimate the background errors and the prior errors relative to each data set. A proper estimation of prior errors is also a necessary condition to reliably estimate the a posteriori uncertainty of the estimated source term. Using such techniques, we retrieve a total released quantity of caesium-137 in the interval 11.6 – 19.3 PBq with an estimated standard deviation range of 15 – 20% depending on the method and the data sets. The “blind” time intervals of the source term have also been strongly mitigated compared to the first estimations with only activity concentration data.

Keywords: Data assimilation, Atmospheric dispersion, Fukushima accident, Source estimation

1. Introduction

1.1. The Fukushima Daiichi accident

On March 11, 2011, 05:46 UTC, a magnitude 9.0 (M_w) undersea megathrust earthquake occurred in the Pacific Ocean and an extremely destructive tsunami hit the Pacific coast of Japan approximately one hour later. These events caused the automatic shut-down of 4 power plants in Japan. Diesel backup power systems should have sustained the reactors cooling process. In Fukushima Daiichi these backup devices were unfortunately inoperative mainly because of the damages caused by the tsunami.

The Fukushima Daiichi NPP has six nuclear reactors. At the time of the earthquake, reactor 4 had been defuelled and reactors 5 and 6 were in a cold shut-down for planned maintenance.

In the hours that followed, the situation quickly became critical. Reactors 1, 2 and 3 experienced at least partial meltdown and hydrogen explosions. Additionally, fuel rods stored in pools in each reactor building began to overheat as water levels in the pools dropped.

All these events caused a massive discharge of radioactive materials in the atmosphere. The total quantities of released radionuclides as well as the time evolution of these releases have to be estimated in order to assess the sanitary and environmental impact of the accident.

Email address: bocquet@cerea.enpc.fr (Marc Bocquet)

Mathieu et al. (2012) used core inventories and in-situ data (pressure and temperature measurements in the reactors and γ -dose rates in the NPP) as well as first available observations over Japan to build a source term, which was used in Korsakissok et al. (2013) to assess the high γ -dose rates zones at a local scale. Chino et al. (2011) used a few activity concentration measurements in the air to calibrate the magnitude of some identified releases of ^{131}I and ^{137}Cs . Katata et al. (2012) and Terada et al. (2012) updated these estimations as new data were available. Stohl et al. (2012) performed an inverse modelling estimation using activity concentrations in the air, as well as deposition data at a global scale to estimate the release of ^{133}Xe and ^{137}Cs . However their estimation was shown to be quite sensitive to the prior information on the source used in the inversion. At the same time, Winiarek et al. (2012b) proposed a method to properly estimate the prior errors to perform inverse modelling using activity concentrations in the air. They applied it to estimate the source terms of ^{131}I and ^{137}Cs .

1.2. Objectives and outline

In Winiarek et al. (2012b) we emphasised the importance of a proper estimation of prior errors in the inverse modelling algorithm. We proposed new methods to estimate two hyper-parameters: the variance of observation errors and the variance of background errors, assuming that all observation errors have the same variance. This assumption is acceptable when using only one type of data in the algorithm. On the other hand the general lack of data in accidental situations stresses the need for algorithms that would use all available data in the same inversion. The first objective of this paper is to extend the methods proposed in Winiarek et al. (2012b) to the simultaneous estimation of prior errors when using different data sets in the inversion. The second objective is to apply these methods to the challenging reconstruction of the caesium-137 source term of the Fukushima Daiichi accident, as well as to obtain an objective uncertainty on this estimation.

In Section 2 we briefly recall the methodology for the inverse modelling of accidental releases of pollutants. The algorithm is sensitive to the statistics of the errors so that we propose methods based on the maximum likelihood principle to estimate these errors. This general maximum likelihood scheme takes into account the positivity of the source and the presence of several types of data.

In Section 3 we apply this new method to the reconstruction of the atmospheric release of ^{137}Cs from the Fukushima Daiichi power plant. The inversions are computed using three data sets: activity concentrations

in the air, daily measurements of deposited material and total cumulated deposition. The new source terms are discussed and compared to earlier estimations. The posterior uncertainties of the retrieved sources are also computed.

Results are summarised and conclusions are given in Section 4.

2. Methodology

2.1. Inverse modelling of accidental releases and estimation of errors

To reconstruct the source term of an accidental release of a pollutant into the atmosphere, inverse modelling techniques are a powerful alternative to a trial and error approach with direct numerical models, which is still widely used in such situations. Inverse modelling techniques can objectively estimate the source term using the information content of an observation set and a numerical model that simulates the dispersion event. The atmospheric transport model (ATM), which is linear in our case for gaseous and particulate matter, provides the relationship between the source term and the observation set through the source-receptor equation

$$\boldsymbol{\mu} = \mathbf{H}\boldsymbol{\sigma} + \boldsymbol{\epsilon}, \quad (1)$$

where $\boldsymbol{\mu}$ in \mathbb{R}^d is the measurement vector, $\boldsymbol{\sigma}$ in \mathbb{R}^N is the source vector, and \mathbf{H} is the Jacobian matrix of the transport model which incorporates the observation operator as well. The vector $\boldsymbol{\epsilon}$ in \mathbb{R}^d , called the observation error in this article, represents the instrumental errors, the representativeness errors and a fraction of model error altogether.

In an accidental context the number of observations is very often limited. Specific meteorological conditions, like during the Fukushima accident, can also lead to a weak observability of a part of the source term. In these cases, the source-receptor relationship defined by Eq. (1) constitutes an ill-posed inverse problem (Winiarek et al., 2011).

One solution to deal with the lack of constraints is to implement parametric methods where the source to retrieve is reduced to a very limited number of parameters. The inverse problem is *de facto* regularised and it can be solved using different techniques, such as stochastic sampling techniques which allow to access the parameters posterior distributions (Delle Monache et al., 2008; Yee et al., 2008). Nevertheless if the true source does not match the parametric model, the inversion may fail or yield a meaningless solution.

Another option is the use of non-parametric methods to retrieve a general source field. This field can be discretised, for example to match the model discretisation, but the number of variables remains large and may still be larger than the number of observations in the data set. The non-parametric approach is robust and flexible since no strong a priori assumptions are made on the source but it has its own constraints. If Gaussian statistics are assumed for observation errors, the inversion relies on the minimisation of the cost function

$$\mathcal{L}(\boldsymbol{\sigma}) = \frac{1}{2} (\boldsymbol{\mu} - \mathbf{H}\boldsymbol{\sigma})^T \mathbf{R}^{-1} (\boldsymbol{\mu} - \mathbf{H}\boldsymbol{\sigma}), \quad (2)$$

where \mathbf{R} is the observation error covariance matrix: $\mathbf{R} = \mathbf{E}[\boldsymbol{\epsilon}\boldsymbol{\epsilon}^T]$, where $\boldsymbol{\epsilon}$ has been defined by Eq. (1). One simple choice is to neglect correlations between observation errors and to take \mathbf{R} diagonal. If all the observations are of the same type, one can even assume that $\mathbf{R} = r^2 \mathbf{I}_d$, r^2 being the variance of the observation errors (\mathbf{I}_d is the identity matrix in $\mathbb{R}^{d \times d}$). With a low number of observations and/or a poor observability of several source term parts, the minimisation of Eq. (2) gives infinitely many solutions. One needs to regularise the inverse problem, usually by adding a Tikhonov term in the cost function:

$$\begin{aligned} \mathcal{L}(\boldsymbol{\sigma}) = & \frac{1}{2} (\boldsymbol{\mu} - \mathbf{H}\boldsymbol{\sigma})^T \mathbf{R}^{-1} (\boldsymbol{\mu} - \mathbf{H}\boldsymbol{\sigma}) \\ & + \frac{1}{2} (\boldsymbol{\sigma} - \boldsymbol{\sigma}_b)^T \mathbf{B}^{-1} (\boldsymbol{\sigma} - \boldsymbol{\sigma}_b). \end{aligned} \quad (3)$$

The solution of the inverse problem is now unique, but two additional (vector and matrix) parameters have been introduced: $\boldsymbol{\sigma}_b$ is the first guess for the source (or background term) and \mathbf{B} is the background error covariance matrix: $\mathbf{B} = \mathbf{E}[(\boldsymbol{\sigma} - \boldsymbol{\sigma}_b)(\boldsymbol{\sigma} - \boldsymbol{\sigma}_b)^T]$.

In an accidental situation and particularly in the Fukushima accident context, the choice of $\boldsymbol{\sigma}_b = \mathbf{0}$ is relevant because (i) many of the parameters are likely to be zero (ii) it guarantees an independent estimate (iii) it avoids the risk of an *inversion crime*, since most of the first guess built by physics models are eventually calibrated using early observations. One can refer to Bocquet (2005); Davoine and Bocquet (2007); Winiarek et al. (2012b) for extended discussions on this choice.

Still in an accidental context, off-diagonal terms in \mathbf{B} are often negligible. For example the γ -dose measurements made in the Fukushima nuclear power plant (NPP) indicate that the source term is probably composed of uncorrelated events¹. This is the reason why we take $\mathbf{B} = m^2 \mathbf{I}_N$ in this article.

¹<http://www.tepco.co.jp/en/nu/monitoring/index-e.html>

As it was shown in the Chernobyl case in Davoine and Bocquet (2007) or in the Fukushima case in Winiarek et al. (2012b) or Stohl et al. (2012), the retrieved source is very sensitive to the matrices \mathbf{R} and \mathbf{B} , hence to the two hyper-parameters r and m . This is the reason why hyper-parameters estimation techniques are required. In Davoine and Bocquet (2007); Krysta et al. (2008); Saide et al. (2011), the L-curve technique of Hansen (1992) was successfully used to estimate the ratio r/m or both parameters. In the recent years several methodological developments in the data assimilation for weather forecast have focused on the estimation of the hyper-parameters of the prior errors. They are mostly based on either cross-validation technique or on the maximum likelihood principle (e.g. Mitchell and Houtekamer, 1999; Chapnik et al., 2004, 2006; Anderson, 2007; Li et al., 2009). These techniques have also been implemented in the context of atmospheric chemistry inverse modelling, using for example the χ^2 criterion (Ménard et al., 2000; Elbern et al., 2007; Davoine and Bocquet, 2007), the maximum likelihood principle (Michalak et al., 2004), or statistical diagnostics (Schwinger and Elbern, 2010).

In Winiarek et al. (2012b) we implemented several methods for the estimation of r and m . One of these methods relies on the L-curve coupled with a χ^2 criterion. Another one is based on the maximum likelihood principle and takes into account without approximation the positivity of the source. This study only exploited activity concentrations in the air. In the case where several types of data are used in the inversion algorithm, the number of hyper-parameters to estimate increases. One can for instance try to estimate one value of the variance of observation errors for each data set, that is an r^2 attached to each data set. This simultaneous estimation of prior errors is the methodological objective of this article.

2.2. Prior errors statistics and cost function minimisation

The observation errors defined by Eq. (1) are assumed normally distributed, with a probability density function (pdf):

$$p_{\boldsymbol{\epsilon}}(\boldsymbol{\epsilon}) = \frac{e^{-\frac{1}{2}\boldsymbol{\epsilon}^T \mathbf{R}^{-1} \boldsymbol{\epsilon}}}{\sqrt{(2\pi)^d |\mathbf{R}|}}, \quad (4)$$

where $|\mathbf{R}|$ is the determinant of the observation error covariance matrix \mathbf{R} . \mathbf{R} is assumed diagonal (it is an approximation as model errors may introduce some correlations). Besides, it is assumed that the errors made on observations of the same type have the same variance, so that if \mathbf{R}_i represents the sub-block of \mathbf{R} relative to the

215 data set i , one has $\mathbf{R}_i = r_i^2 \mathbf{I}_{d_i}$, where d_i is the number of
 216 observations in data set i ($\sum_{i=1}^{N_d} d_i = d$, N_d is the number
 217 of different data sets) and r_i^2 is the corresponding error
 218 variance. Note that due to the limited number of obser-
 219 vations and in order to avoid a too severely undercon-
 220 strained problem, it is essential to keep the number of
 221 hyper-parameters that define \mathbf{R} as small as possible (N_d
 222 hyper-parameters in our case: $(r_i)_{1 \leq i \leq N_d}$). For instance,
 223 an approach such as the one put forward by Desroziers
 224 et al. (2005) or Schwinger and Elbern (2010) is likely to
 225 be unaffordable in this accidental context.

226 As far as background errors are concerned, we could
 227 also use Gaussian statistics. The advantages of this
 228 choice would be analytical solutions for both the source
 229 term estimation and the related uncertainty based on the
 230 Best Linear Unbiased Estimator (BLUE) theory. How-
 231 ever, such a Gaussian assumption could lead to negative
 232 values in the retrieved source term, because of the lack
 233 of sufficient observations to constrain the source term.
 234 To avoid non-physical results, truncated normal statis-
 235 tics for background errors are considered, enforcing the
 236 positivity of the retrieved source term. It is known
 237 to provide valuable information to the data assimila-
 238 tion system (Bocquet et al., 2010) and was successfully
 239 used in the context of the Fukushima Daiichi accident
 240 (Winiarek et al., 2012b). The corresponding pdf of this
 241 normalised truncated normal distribution reads in the
 242 general case

$$\begin{cases} \text{if } \boldsymbol{\sigma} \geq \mathbf{0} & p(\boldsymbol{\sigma}) = \left(\int_{s \geq \mathbf{0}} e^{-\frac{1}{2}(s-\boldsymbol{\sigma}_b)^T \mathbf{B}^{-1}(s-\boldsymbol{\sigma}_b)} ds \right)^{-1} \\ & \times e^{-\frac{1}{2}(\boldsymbol{\sigma}-\boldsymbol{\sigma}_b)^T \mathbf{B}^{-1}(\boldsymbol{\sigma}-\boldsymbol{\sigma}_b)} \\ \text{otherwise} & p(\boldsymbol{\sigma}) = 0. \end{cases} \quad (5)$$

243 The normalisation factor can be simplified in our case
 244 where \mathbf{B} is diagonal and $\boldsymbol{\sigma}_b = \mathbf{0}$ to yield the following
 245 semi-Gaussian pdf:

$$\begin{cases} \text{if } \boldsymbol{\sigma} \geq \mathbf{0} & p(\boldsymbol{\sigma}) = \frac{e^{-\frac{1}{2}\boldsymbol{\sigma}^T \mathbf{B}^{-1} \boldsymbol{\sigma}}}{\sqrt{(\pi/2)^N |\mathbf{B}|}} \\ \text{otherwise} & p(\boldsymbol{\sigma}) = 0, \end{cases} \quad (6)$$

246 where $|\mathbf{B}|$ is the determinant of the background error co-
 247 variance matrix \mathbf{B} .

248 Bayes' rule helps to formulate the inference, after the
 249 acquisition of the measurement vector $\boldsymbol{\mu}$:

$$\begin{aligned} p(\boldsymbol{\sigma}|\boldsymbol{\mu}) &= \frac{p(\boldsymbol{\mu}|\boldsymbol{\sigma})p(\boldsymbol{\sigma})}{p(\boldsymbol{\mu})} = \frac{p_e(\boldsymbol{\mu} - \mathbf{H}\boldsymbol{\sigma})p(\boldsymbol{\sigma})}{p(\boldsymbol{\mu})} \\ &\propto \exp \left\{ -\frac{1}{2}(\boldsymbol{\mu} - \mathbf{H}\boldsymbol{\sigma})^T \mathbf{R}^{-1}(\boldsymbol{\mu} - \mathbf{H}\boldsymbol{\sigma}) \right. \\ &\quad \left. -\frac{1}{2}\boldsymbol{\sigma}^T \mathbf{B}^{-1} \boldsymbol{\sigma} \right\} \mathbb{I}_{\boldsymbol{\sigma} \geq \mathbf{0}}, \end{aligned} \quad (7)$$

250 where $\mathbb{I}_{\boldsymbol{\sigma} \geq \mathbf{0}}$ is equal to 1 when $\boldsymbol{\sigma}_i \geq 0$, for every $i \leq N$.
 251 Otherwise its value is 0.

252 From this inference, the source term is estimated us-
 253 ing the maximum a posteriori estimator (MAP), denoted
 254 $\boldsymbol{\sigma}_a$:

$$\boldsymbol{\sigma}_a = \underset{\boldsymbol{\sigma}}{\operatorname{argmax}} p(\boldsymbol{\sigma}|\boldsymbol{\mu}). \quad (8)$$

255 Maximising $p(\boldsymbol{\sigma}|\boldsymbol{\mu})$ is equivalent to maximising
 256 $\ln p(\boldsymbol{\sigma}|\boldsymbol{\mu})$, which is equivalent to maximising the term
 257 in the exponential under the constraint of positivity,
 258 which is ultimately equivalent to minimising cost func-
 259 tion Eq. (3) under the constraint of positivity. Since
 260 there is no analytical solution to this problem, the posi-
 261 tivity of $\boldsymbol{\sigma}$ should be enforced during the numerical
 262 minimisation which is performed with a bounded quasi-
 263 Newton algorithm (Byrd et al., 1995).

264 In practice, because of the low number of observa-
 265 tions, the estimated source term is very sensitive to the
 266 matrices \mathbf{R} and \mathbf{B} , i.e. to the hyper-parameters $(r_i)_{1 \leq i \leq N_d}$
 267 and m . This is the reason why we have to estimate these
 268 parameters rigorously. We propose to extend the meth-
 269 ods developed in Winiarek et al. (2012b) to the use of
 270 several different data sets by simultaneously estimating
 271 the respective hyper-parameters.

272 2.3. Estimation of hyper-parameters

273 2.3.1. Unapproximated maximum likelihood values 274 screening

275 The estimation of the prior errors' magnitude pro-
 276 posed in this section relies on the maximum likelihood
 277 paradigm (Dee, 1995). As the prior probabilities depend
 278 on the hyper-parameters, the likelihood of the observa-
 279 tion set, which can be written

$$p(\boldsymbol{\mu}|\boldsymbol{\theta}) = \int d\boldsymbol{\sigma} p(\boldsymbol{\mu}|\boldsymbol{\sigma}; \boldsymbol{\theta}) p(\boldsymbol{\sigma}|\boldsymbol{\theta}), \quad (9)$$

280 is a function of the hyper-parameters vector
 281 $\boldsymbol{\theta} = (r_1, \dots, r_{N_d}, m)^T$. The pdfs $p(\boldsymbol{\mu}|\boldsymbol{\sigma}; \boldsymbol{\theta})$ and
 282 $p(\boldsymbol{\sigma}|\boldsymbol{\theta})$ are the prior pdfs defined by Eq. (4) and Eq. (6).
 283 If it exists, the vector $\boldsymbol{\theta}$ that maximises $p(\boldsymbol{\mu}|\boldsymbol{\theta})$ is the
 284 most likely vector of hyper-parameters consistent with
 285 the observation set $\boldsymbol{\mu}$.

286 The most direct way to estimate these optimal hyper-
 287 parameters is to screen the likelihood function for a
 288 range of values of $\boldsymbol{\theta}$. With our hypothesis on the errors
 289 statistics, the covariance matrices and the first guess, the
 290 likelihood can be written:

$$\begin{aligned} p(\boldsymbol{\mu}|\boldsymbol{\theta}) &= \frac{e^{-\frac{1}{2}\boldsymbol{\mu}^T (\mathbf{R} + \mathbf{H}\mathbf{B}\mathbf{H}^T)^{-1} \boldsymbol{\mu}}}{\sqrt{(2\pi)^d |\mathbf{H}\mathbf{B}\mathbf{H}^T + \mathbf{R}|}} \\ &\times \int_{\boldsymbol{\sigma} \geq \mathbf{0}} \frac{e^{-\frac{1}{2}(\boldsymbol{\sigma} - \boldsymbol{\sigma}_{\text{BLUE}})^T \mathbf{P}_{\text{BLUE}}^{-1}(\boldsymbol{\sigma} - \boldsymbol{\sigma}_{\text{BLUE}})}}{\sqrt{(\pi/2)^N |\mathbf{P}_{\text{BLUE}}|}} d\boldsymbol{\sigma}, \end{aligned} \quad (10)$$

291 where σ_{BLUE} is the BLUE estimator, which in our case 331
 292 reads:

$$\sigma_{\text{BLUE}} = \mathbf{B}\mathbf{H}^T(\mathbf{R} + \mathbf{H}\mathbf{B}\mathbf{H}^T)^{-1}\boldsymbol{\mu}, \quad (11)$$

293 and \mathbf{P}_{BLUE} is the corresponding analysis error covariance 332
 294 matrix:

$$\mathbf{P}_{\text{BLUE}} = \mathbf{B} - \mathbf{B}\mathbf{H}^T(\mathbf{R} + \mathbf{H}\mathbf{B}\mathbf{H}^T)^{-1}\mathbf{H}\mathbf{B}. \quad (12)$$

295 The integral term in Eq. (10) has no analytical solu- 333
 296 tion, but can be numerically computed using a stochas- 334
 297 tic method, such as the GHK simulator from Hajivassil-
 298 iou et al. (1996). Nevertheless, if the dimension of $\boldsymbol{\theta}$ is
 299 high, the size of the space to screen can lead to a costly
 300 computation.

301 For details about the calculation of the likelihood ex- 335
 302 pression, and in particular the general case expression, 336
 303 and for details about the use of the GHK simulator to 337
 304 estimate the integral of a truncated normal distribution, 338
 305 one can refer to Winiarek et al. (2012b) and Winiarek 339
 306 et al. (2012a).

307 As a statistical consistent method, we considered it as 340
 308 our reference method, denoted ML in this study. Faster 341
 309 but approximate alternatives can nonetheless be con- 342
 310 sidered and tested against this statistically consistent 343
 311 method.

312 2.3.2. Iterative scheme à-la-Desroziers

313 As an alternative to the costly computation of the 345
 314 likelihood, the use of an iterative scheme which would 346
 315 quickly converge to the maximum likelihood is relevant. 347
 316 In Winiarek et al. (2012b) we used such an iterative 348
 317 algorithm for the estimation of two hyper-parameters. 349
 318 This iterative algorithm was shown to converge to a 350
 319 fixed-point that corresponds, in the context of Gaussian 351
 320 statistics, to the pair of hyper-parameters of maximum 352
 321 likelihood. This algorithm is only an approximation in 353
 322 the context of semi-Gaussian statistics but it yielded ac- 354
 323 ceptable, through slightly different, results. Building on 355
 324 Desroziers and Ivanov (2001) we propose an extension 356
 325 of this online tuning scheme to the simultaneous esti- 357
 326 mation of several prior errors variances. The formulae 358
 327 read:

$$m^2 = \frac{2J_b(\sigma_a)}{N - \text{tr}(\mathbf{P}_{\text{BLUE}}\mathbf{B}^{-1})}, \quad (13)$$

$$r_i^2 = \frac{2J_{oi}(\sigma_a)}{d_i - \text{tr}(\mathbf{H}_i\mathbf{P}_{\text{BLUE}}\mathbf{H}_i^T\mathbf{R}_i^{-1})}, \quad (14)$$

328 where \mathbf{H}_i and \mathbf{R}_i are the sub-blocks of respectively the 330
 329 Jacobian matrix \mathbf{H} and the observation error covariance
 330 matrix \mathbf{R} related to data set i , whose observation vector

is noted $\boldsymbol{\mu}_i$. \mathbf{P}_{BLUE} is defined by Eq. (12). J_b and J_{oi} are
 defined by:

$$J_b(\boldsymbol{\sigma}) = \frac{1}{2}\boldsymbol{\sigma}^T\boldsymbol{\sigma}, \quad (15)$$

$$J_{oi}(\boldsymbol{\sigma}) = \frac{1}{2}(\boldsymbol{\mu}_i - \mathbf{H}_i\boldsymbol{\sigma})^T(\boldsymbol{\mu}_i - \mathbf{H}_i\boldsymbol{\sigma}). \quad (16)$$

The source vector σ_a is obtained from the minimisation
 of the cost function:

$$\mathcal{L}(\boldsymbol{\sigma}) = \frac{J_b(\boldsymbol{\sigma})}{m^2} + \sum_{i=1}^{N_d} \frac{J_{oi}(\boldsymbol{\sigma})}{r_i^2} \quad (17)$$

under the constraint $\boldsymbol{\sigma} \geq \mathbf{0}$. These equations can be used
 in an iterative scheme which we shall call Desroziers'
 scheme later on. This algorithm quickly converges (3-4
 iterations here) to a fixed-point giving estimated hyper-
 parameters and the related source term.

340 3. Applications to the Fukushima accident

341 3.1. Observations

In order to illustrate the proposed methods, observa-
 tions from three different data sets will be considered:

- The activity concentration in the air over Japan
 as described and referred to in Winiarek et al.
 (2012b). This data set contains 104 observations.
- Starting from 18 March 2011, daily measurements
 of deposited ^{137}Cs in 22 prefectures, which repre-
 sents a total of 198 observations².
- Measurements of total deposited ^{137}Cs in an area
 near the NPP (approximately 100 km around).
 Among the 2180 deposition measurements pro-
 vided by the Ministry of Education, Culture,
 Sports, Science and Technology (MEXT) during
 May and June 2011³, 16 were filtered out because
 they are impacted by near-field effects that are not
 represented by larger scale ATMs, so that 2164 ob-
 servations, that are distant enough from the NPP,
 were considered. As shown in Fig. 5(a), they are
 densely distributed in space, but on the downside
 there is no scale of time in these observations.

²<http://www.mext.go.jp/english/incident/1305529.htm>

³http://www.mext.go.jp/b_menu/shingi/chousa/gijyutu/017/shiryo/_icsFiles/afielddfile/2011/09/02/1310688_1.pdf

362 The distribution of the observation sites led to use a
 363 mesoscale domain approximately covering Japan. Be-
 364 cause of the spatial extension and density of the sites,
 365 and because of the frequency of the observations, the
 366 ATM needs a rather limited simulation domain with
 367 high resolution in space and in time.

368 3.2. Modelling the atmospheric dispersion

369 3.2.1. Meteorological fields

370 ECMWF meteorological fields with a spatial resolu-
 371 tion of $0.25^\circ \times 0.25^\circ$ and a temporal resolution of 3 hours
 372 are too coarse to be used for our need. That is the rea-
 373 son why we computed mesoscale meteorological fields
 374 with the Weather Research and Forecasting (WRF) nu-
 375 merical model (Skamarock et al., 2008). The main ob-
 376 jective is to obtain meteorological fields with a spatial
 377 resolution of approximately 5 km and a temporal reso-
 378 lution of 1 h. The computed meteorological fields are
 379 inputs for the atmospheric transport model. Physical
 380 parametrisations as well as the design of simulation do-
 381 mains are summarised in Tab. 1 and the simulation do-
 382 mains are displayed in Fig. 1. One of the key feature
 383 is the use of several thousands of meteorological obser-
 384 vations to constrain the meteorological fields through
 385 nudging techniques (Stauffer and Seaman, 1994).

386 As shown in Fig. 2, WRF simulations show a good
 387 ability to model the occurrence of rain episodes but have
 388 the general tendency to overestimate precipitation rates
 389 (Katata et al. (2012) observed the same behaviour using
 390 MM5). This bias is a severe drawback when looking at
 391 deposition processes as this study aims to do. To avoid
 392 overestimating wet deposition, we used ground obser-
 393 vations of rain rates in Fukushima and Ibaraki prefec-
 394 tures to compute a global debiasing coefficient, that we
 395 found equal to 2.4, by which were divided all precipita-
 396 tion rates computed by the WRF model. We have also
 397 tested local corrections of the precipitation fields using
 398 data assimilation techniques but we did not find them to
 399 be as robust and reliable as a simpler global debiasing
 400 correction.

401 3.2.2. Atmospheric transport model

402 The simulations of the dispersion of radionuclides
 403 from the Fukushima Daiichi nuclear power plant have
 404 been performed with the chemistry-transport model Po-
 405 LAIR3D, the Eulerian model of the POLYPHEMUS platform.
 406 It has been validated for the simulation of radionuclides
 407 transport on the European Tracer Experiment, on the Al-
 408 geciras incident and on the Chernobyl accident (Quélo
 409 et al., 2007).

410 The model integrates the concentration field c of
 411 ^{137}Cs , following the transport equation

$$\frac{\partial c}{\partial t} + \text{div}(\mathbf{u}c) = \text{div}\left(\rho \mathbf{K} \nabla \left(\frac{c}{\rho}\right)\right) - \Lambda^s c - \Lambda^d c + \sigma \quad (18)$$

412 where ρ is the air density, Λ^s is the scavenging rate, Λ^d
 413 represents the radioactive decay and σ is the point-wise
 414 source. \mathbf{K} is the matrix of turbulent diffusion, diagonal
 415 in practice. The vertical component is given by K_z , com-
 416 puted with Louis parametrisation (Louis, 1979). The
 417 horizontal component K_H is taken constant. The bound-
 418 ary condition on the ground is

$$K_z \nabla c \cdot \mathbf{n} = -v^{\text{dep}} c \quad (19)$$

419 where \mathbf{n} is the upward oriented unitary vector, and v^{dep}
 420 is the dry deposition velocity of ^{137}Cs .

421 Two domains of simulation are considered. The finest
 422 domain of simulation is a mesoscale domain covering
 423 Japan, from 131.03°E to 144.53°E and from 30.72°N to
 424 43.72°N with a spatial resolution of $0.05^\circ \times 0.05^\circ$. The
 425 number of grid points in this domain is 270×260 . Be-
 426 cause of the small size of the domain there is a risk of
 427 re-circulation of the plume outside the domain so that
 428 the model could fail to account for radionuclides re-
 429 entries. To avoid such situation and in order to com-
 430 pute the boundary conditions to this domain by a nest-
 431 ing technique, another more extended domain of sim-
 432 ulation with a coarser resolution is used. It covers a
 433 region from 115.03°E to 165.03°E and from 25.02°N to
 434 60.02°N with a resolution of $0.25^\circ \times 0.25^\circ$. This con-
 435 figuration is displayed in Fig. 1. For both domains the
 436 POLAIR3D model is configured with 15 vertical levels
 437 ranging from 0 to 8000 m.

438 Caesium-137 is modelled as monodispersed passive
 439 particulate matter with a radioactive decay of 11000
 440 days. Dry deposition is modelled using a simple scheme
 441 with a constant deposition velocity: $v^{\text{dep}} = 0.15 \text{ cm.s}^{-1}$
 442 (Bocquet, 2012) over land, and $v^{\text{dep}} = 0.01 \text{ cm.s}^{-1}$ over
 443 the ocean (see Estournel et al. (2012) and references
 444 within). As far as wet deposition is concerned, the
 445 parametrisation used in this study is a below-cloud scav-
 446 enging scheme of the form:

$$\Lambda^s = a \left(\frac{p}{p_0}\right)^b \quad (20)$$

447 where p stands for the precipitation rate and $p_0 =$
 448 1 mm.h^{-1} , a and b being two constants respectively
 449 equal to $8.4 \cdot 10^{-5} \text{ s}^{-1}$ and 0.79 following Maryon et al.
 450 (1991).

Table 1: Configuration and physical parametrisations of the WRF model. A two-way nesting technique is used between domain 1 and domain 2.

Domain	1	2
Spatial resolution	18 km	6 km
Number of grid points	340 × 250	241 × 241
Number of vertical levels	27	27
Numerical time-step	60 s	20 s
Output time-step	3600 s	3600 s
Planetary boundary layer	Yonsei University	Yonsei University
Micro-physics	Kessler	WRF Single Moment 3
Cumulus physics	Grell-Devenyi	Grell-Devenyi
Longwave radiation	RRTM	RRTM
Shortwave radiation	Dudhia	Dudhia
Surface layer	MM5 similarity	MM5 similarity
Land surface	Noah LSM	Noah LSM
Nudging	Grid nudging	Grid nudging

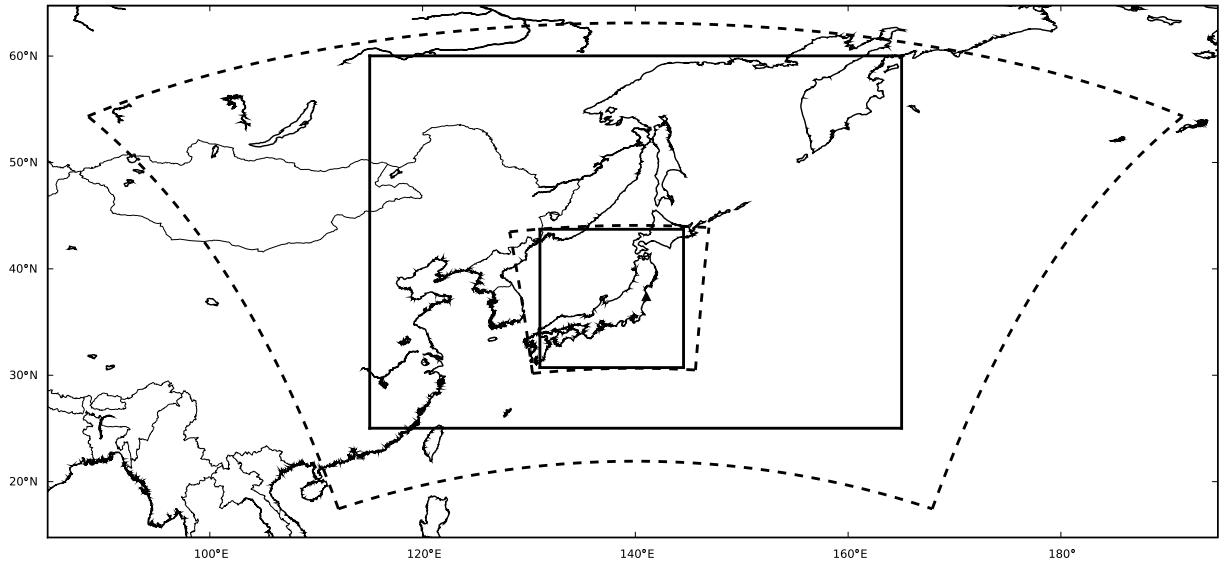


Figure 1: Map of the simulation domains used in WRF (dashed-line domains) and in POLAIRD3D (full-line domains). Two-way nesting is used in the WRF simulations and one-way nesting in the POLAIRD3D simulation. A triangle marks the location of the Fukushima Daiichi nuclear power plant.

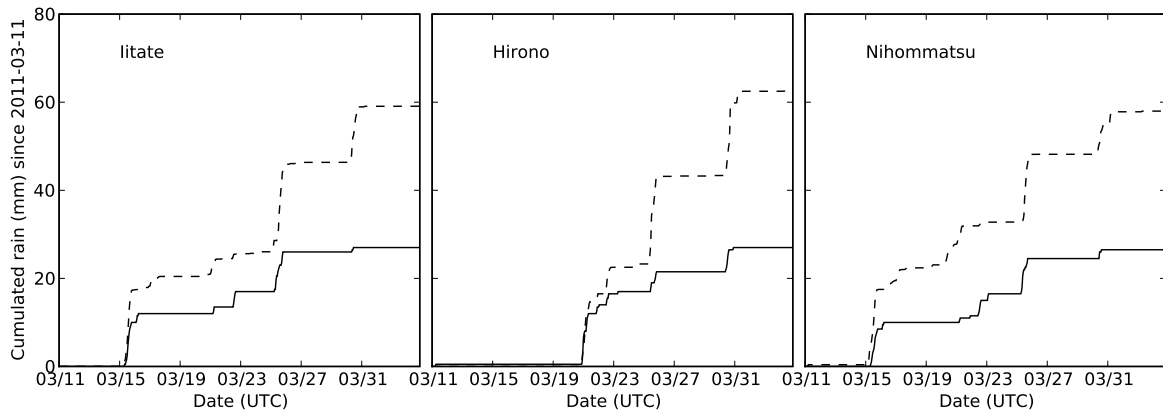


Figure 2: Comparison between WRF calculations (dashed lines) and observations (full lines) for cumulated precipitation (in mm) at some surface weather stations in Fukushima prefecture.

451 The advection is implemented thanks to a third-order 483
 452 direct space-time scheme, with a Koren-Sweby flux limiter 484
 453 function. Because of the plume sharp gradients, it 485
 454 is important that such a limiter is used. The diffusion 486
 455 scheme is integrated through an implicit second-order 487
 456 Rosenbrock scheme, with a three-point spatial scheme, 488
 457 and directional splitting. 489

458 This study attempts to reconstruct the source term 490
 459 from March 11 to April 1 (which represents $N = 504$ 491
 460 one-hour time-steps). However the simulations run over 492
 461 a longer period (from March 11 to April 5) in order to 493
 462 exploit the information content of later observations. A 494
 463 total of 504 direct simulations are thus performed to fill 495
 464 the Jacobian matrix \mathbf{H} column by column, and no ad- 496
 465 joint model is needed in this process following Abida 497
 466 and Bocquet (2009); Winiarek et al. (2011). 498

467 3.3. Inverse modelling results only using activity con- 500 468 centrations in the air 501

469 The proposed methods can of course be applied to in- 502
 470 verse modelling using only one data set, such as activity 503
 471 concentration in the air data (the first data set described 504
 472 in Section 3.1 and which contains 104 observations). In 505
 473 this case, the formulae are rigorously equivalent to the 506
 474 ones presented in Winiarek et al. (2012b). It is nonethe- 507
 475 less interesting to perform such inversion. It allows to 508
 476 check and confirm the consistency of the model, even 509
 477 though the meteorological fields and the removal pro- 510
 478 cesses parameterisations are different.

479 3.3.1. Estimation of parameters and total released ac- 512 480 tivity 513

481 The estimated hyper-parameters and the estimated to- 514
 482 tal released activities are reported in Tab. 2 together with 515

483 results found in Winiarek et al. (2012b) using the same 484
 485 data set. The estimated hyper-parameters as well as the 486
 487 total released activities in the case of the ML method are 488
 489 close and confirm the consistency of this approach.

489 As discussed in Winiarek et al. (2012b) Desroziers' 490
 491 scheme is based on Gaussian assumptions and thus has 492
 492 to be considered an approximation in the case of semi- 493
 493 Gaussian assumptions for background errors statistics. In 494
 494 the situation where only few data are available it could 495
 495 yield results different from the maximum likelihood 496
 496 estimation. Nevertheless the gap here is smaller than 497
 497 it was in Winiarek et al. (2012b) with the same data. It 498
 498 may be caused by the use of a mesoscale model with a 499
 499 better resolution in space and in time which increases 500
 500 the general consistency in the system. The clear de- 501
 501 crease of r , that represents the magnitude of the ob- 502
 502 servational error, including representativeness error and 503
 503 part of model error, was to be expected and may be due 504
 504 to a better resolved model hence reducing the impact of 505
 505 model error in the inversion. 506

506 Using the maximum likelihood estimation, the total 507
 507 released activity of ^{137}Cs is estimated to be 1.1×508
 508 10^{16} Bq. This is consistent with other estimations: 509
 509 1.2×10^{16} Bq for Winiarek et al. (2012b) and Chino 510
 510 et al. (2011), 1.3×10^{16} Bq for Terada et al. (2012),
 510 1.6×10^{16} Bq for Saunier et al. (2013), 2.1×10^{16} Bq
 510 for Mathieu et al. (2012) or 3.6×10^{16} Bq for Stohl et al.
 510 (2012).

511 3.3.2. Temporal profile and uncertainty reduction 512

512 Due to the meteorological conditions which have of- 513
 513 ten transported the radionuclides towards the Pacific 514
 514 Ocean, and to the low number of activity concentration 515
 515 data, the observability of the plume is reduced. That is

Table 2: Estimation of parameters and corresponding reconstructed released activity for caesium-137 source reconstruction using only activity concentration observations in the air.

parameter	method	Regional scale model Winiarek et al. (2012b)	Mesoscale model This study
r (Bq m ⁻³)	Desroziers' scheme	5.4	2.1
	Maximum likelihood	3.3	1.9
m (Bq s ⁻¹)	Desroziers' scheme	5.3×10^{10}	8.9×10^{10}
	Maximum likelihood	2.0×10^{11}	1.6×10^{11}
Released activity (Bq)	Desroziers' scheme	3.3×10^{15}	7.2×10^{15}
	Maximum likelihood	1.2×10^{16}	1.1×10^{16}

516 why inverse modelling methods are only able to recon- 555
517 struct the source term in some specific time intervals. 556
518 Consequently the estimated total released activities have 557
519 to be considered as lower bound estimates of the actual 558
520 releases. 559

521 The reconstructed source term and its uncertainty are 560
522 displayed in Fig. 3(a). The posterior uncertainty has 561
523 been computed from a Monte Carlo analysis, where the 562
524 observations and the background term are perturbed us- 563
525 ing their prior errors definition and the hyper-parameters 564
526 estimates (2×10^4 draws and inversions are performed). 565
527 Then the standard deviation of the estimators ensemble 566
528 is used to estimate the posterior uncertainty of the re- 567
529 constructed source term. The uncertainty on the total 568
530 released activity is around 65%. 569

531 The time intervals of observability are clearly visible 571
532 in the shape of the uncertainty. Three periods are par- 572
533 ticularly well observed: the first one lies approximately 573
534 from 14 March to 15 March, the second one lies from 574
535 19 March to 22 March and the last one from 24 March 575
536 to 26 March. Once again the temporal profiles of the 576
537 source term and its uncertainty are very consistent with 577
538 the inversion made in Winiarek et al. (2012b). 578

539 Compared to source term estimates constructed from 578
540 in-situ events monitoring and core inventories (Mathieu 579
541 et al., 2012), a few events are not retrieved: the first 580
542 hydrogen explosions in Unit 1 on 12 March, the vent- 581
543 ings of Unit 3 on 13 March and the events concerning 582
544 Unit 2 and 3 on 16 March and 18 March. On the other 583
545 hand, the multiple events of 14 March and 15 March are 584
546 present in the reconstructed source term, even though in 585
547 an incomplete way since the last release, probably be- 586
548 tween 7:00 UTC and 12:00 UTC on 15 March, is miss- 587
549 ing. This release is partly accounting for the north-west 588
550 pattern on the deposition map, but no activity concen- 589
551 tration observation is available to help reconstruct this 590
552 event. The releases of 20 March and the ones from 21
553 March to 23 March are also retrieved. As far as the re-
554 lease around 25 March is concerned, there seems to be

a slight offset of 12 hours in the reconstruction. The re-
leases reconstructed on 19 March are not mentioned by
these inventories, but seem compatible with the in-situ
measurements of γ -dose rates from operator TEPCO⁴,
for example on the northside of main office or near the
west gate of the NPP. They are also retrieved by Stohl
et al. (2012). They precede the attempts of emergency
cooling with Tokyo Fire Department means. Finally, the
releases around 30 March, not mentioned by the former
inventories, are also retrieved by Terada et al. (2012).

The scatter plot of all observations is displayed in
Fig. 4(a). The simulation using the source term re-
constructed with activity concentration data only does
not show any systematic bias when estimating the de-
posited activities. Again, this shows the consistency
of the model and in particular of the removal processes
(wet and dry deposition).

3.4. Results of the inverse modelling using the three raw data sets

The total deposited ¹³⁷Cs measurements offer no in-
formation about the time of deposition as they are mea-
surements performed a posteriori, in May and June
2011. When only these measurements are used to
attempt reconstructing the source term, the total re-
leased estimated activity seems consistent (between
 1.1×10^{16} Bq and 1.2×10^{16} Bq). However, the tem-
poral profile, displayed in Fig. 3(b), is highly doubtful.
Only releases on 23 and on 25 March are clearly visi-
ble. Indeed, the system has too much freedom to fit the
data. The only constraint is the background term in the
cost function, which in the case where the first guess
is taken null (as we do) only defines a scale of ampli-
tude. Therefore, even if these observations are abun-
dant with a good spatial distribution, we propose in the
next sections to jointly use them with other measure-
ments with a good temporal resolution, such as activity

⁴<http://www.tepco.co.jp/en/nu/monitoring/index-e.html>

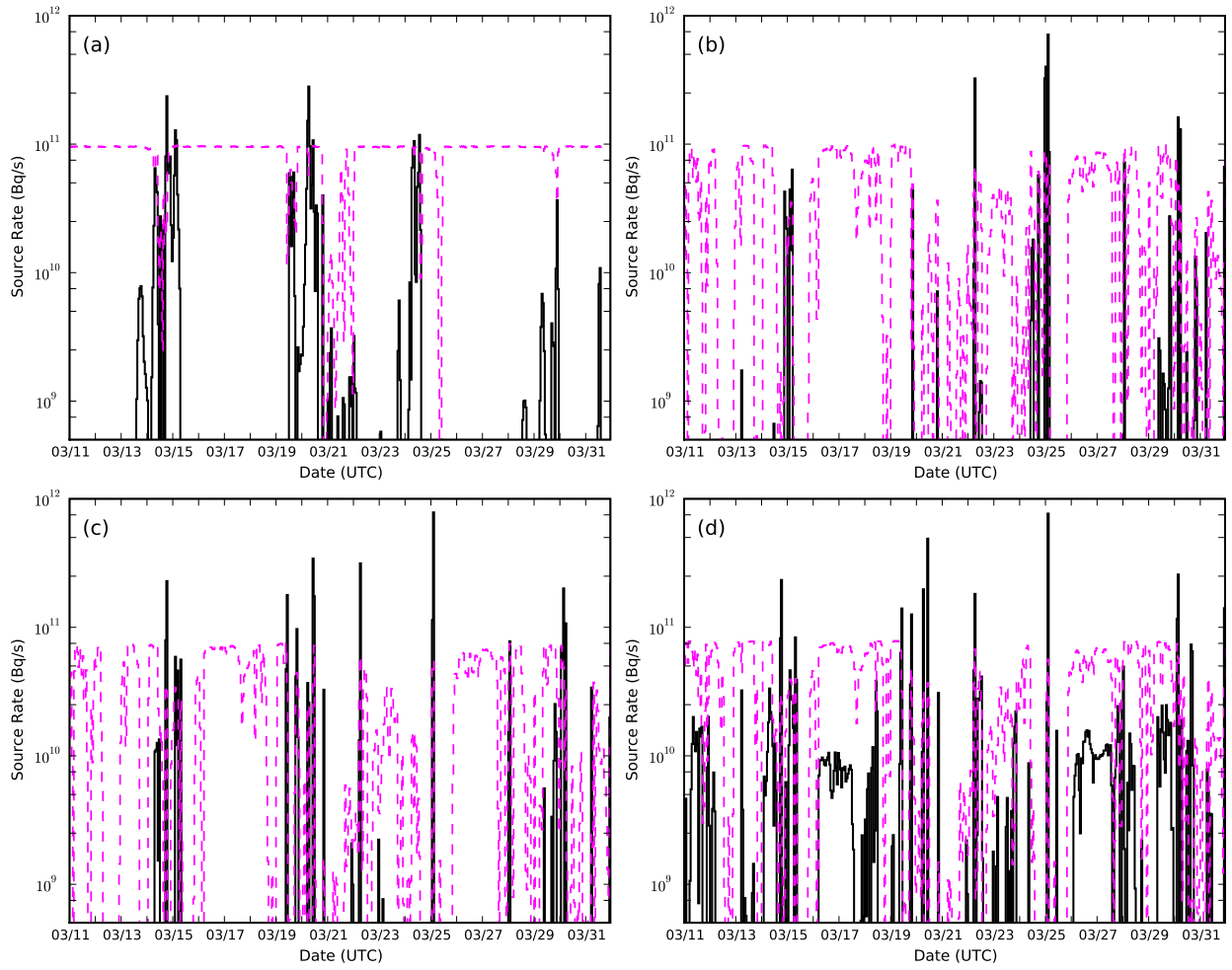


Figure 3: Full line: Temporal profile of reconstructed caesium-137 source term using (a): activity concentration of ^{137}Cs measurements in the air only, (b): total cumulated deposited ^{137}Cs measurements only, (c): the activity concentration in the air, the daily fallout measurements and the total cumulated deposition raw measurements, (d): the activity concentration in the air, the daily fallout measurements and the super-observations computed from the total cumulated deposited ^{137}Cs . Dashed lines: posterior uncertainty of the source term computed using a Monte Carlo simulation.

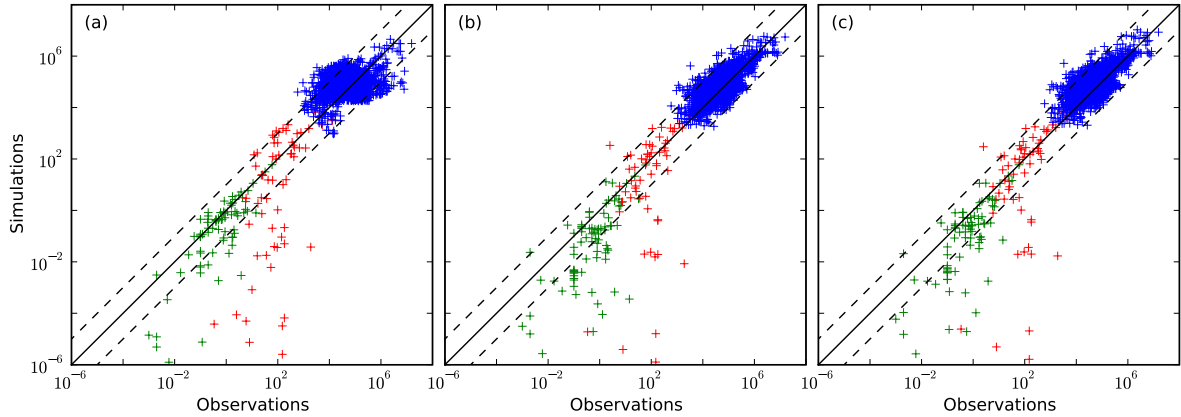


Figure 4: Scatter plots of ^{137}Cs activity concentration in the air (green crosses in Bq m^{-3}), daily measurements of deposited ^{137}Cs (red crosses in Bq m^{-2}) and total cumulated deposited ^{137}Cs (blue crosses in Bq m^{-2}). (a) inversion only using activity concentrations in the air. (b) inversion using the three raw data sets. (c) inversion using the three data sets including super-observations. The dashed lines represent a misfit of a factor 10 between observations and modelled values.

591 concentrations in the air and daily measurements of de- 621
 592 posited material. Consequently we propose to use the 622
 593 three data sets described in Section 3.1 in the same in- 623
 594 version. In this aim the prior errors have to be estimated 624
 595 simultaneously for the background and the three data 625
 596 sets ($N_d = 3$). 626

597 3.4.1. Estimation of parameters and total released ac- 628 598 tivity 629

599 As expected, when the number of available obser- 630
 600 vations increases, the results yielded by Desroziers' 631
 601 scheme tend to get closer to the maximum likelihood 632
 602 estimation. 633

603 The estimated hyper-parameters as well as the esti- 634
 604 mated total released activities are reported in Tab. 3. 635
 605 Excepted for the daily measurements hyper-parameter, 636
 606 the values of estimated hyper-parameters do not differ 637
 607 much when using Desroziers' scheme or the maximum 638
 608 likelihood method. 639

609 Using these data sets, the total released activity of 640
 610 ^{137}Cs is estimated to be between 1.2×10^{16} Bq and 641
 611 1.3×10^{16} Bq. 642

612 3.4.2. Temporal profile and uncertainty reduction 643

613 The reconstructed source term and its uncertainty are 644
 614 displayed in Fig. 3(c). 645

615 The observability of the accident is improved com- 646
 616 pared to the inversion using only activity concentrations 647
 617 in the air. The time windows where the uncertainty is 648
 618 reduced are much larger, specially before 14 March and 649
 619 between 19 March and 26 March. The uncertainty on 650
 620 the total released activity has been reduced from around 651

65% when using only activity concentration to around 621
 25% in this case. 622

623 The events that were retrieved in the first inversion 624
 625 are still reconstructed with this data set. The time offset 626
 627 on the release of 25 March has disappeared. The system 628
 629 is now able to reconstruct the late release of 15 March, 630
 631 from 7:00 UTC to 9:00 UTC and hence to model the 632
 633 north-west pattern of deposited ^{137}Cs . The maps of ob- 634
 635 served and simulated total deposition are displayed in 636
 637 Fig. 5(a,b,c,d). 638

639 3.5. Results of the inverse modelling using super- 640 641 observations computed from the three raw data 642 643 sets 644

645 As mentioned above, measurements of the third data 646
 647 set are very densely distributed. This proximity cer- 648
 649 tainly induces correlations in the observation errors 649
 650 (mainly through model errors) that are not taken into ac- 650
 651 count in our system. One way to take into account these 651
 correlations would be to use a non-diagonal \mathbf{R} matrix. This method would increase the computation cost as the inverse of \mathbf{R} is needed for the minimisation of the cost function Eq. (3). Besides, this would introduce additional hyper-parameters in the correlation model which would have to be properly estimated as well. Such an estimation could be a difficult task in a situation with a low number of observations. Another route that can be chosen to deal with densely distributed data is the thinning of observations which consists in the optimal selection of observations. These techniques are already used in the assimilation of satellite data in the weather forecast community (Liu and Rabier, 2002). Yet another

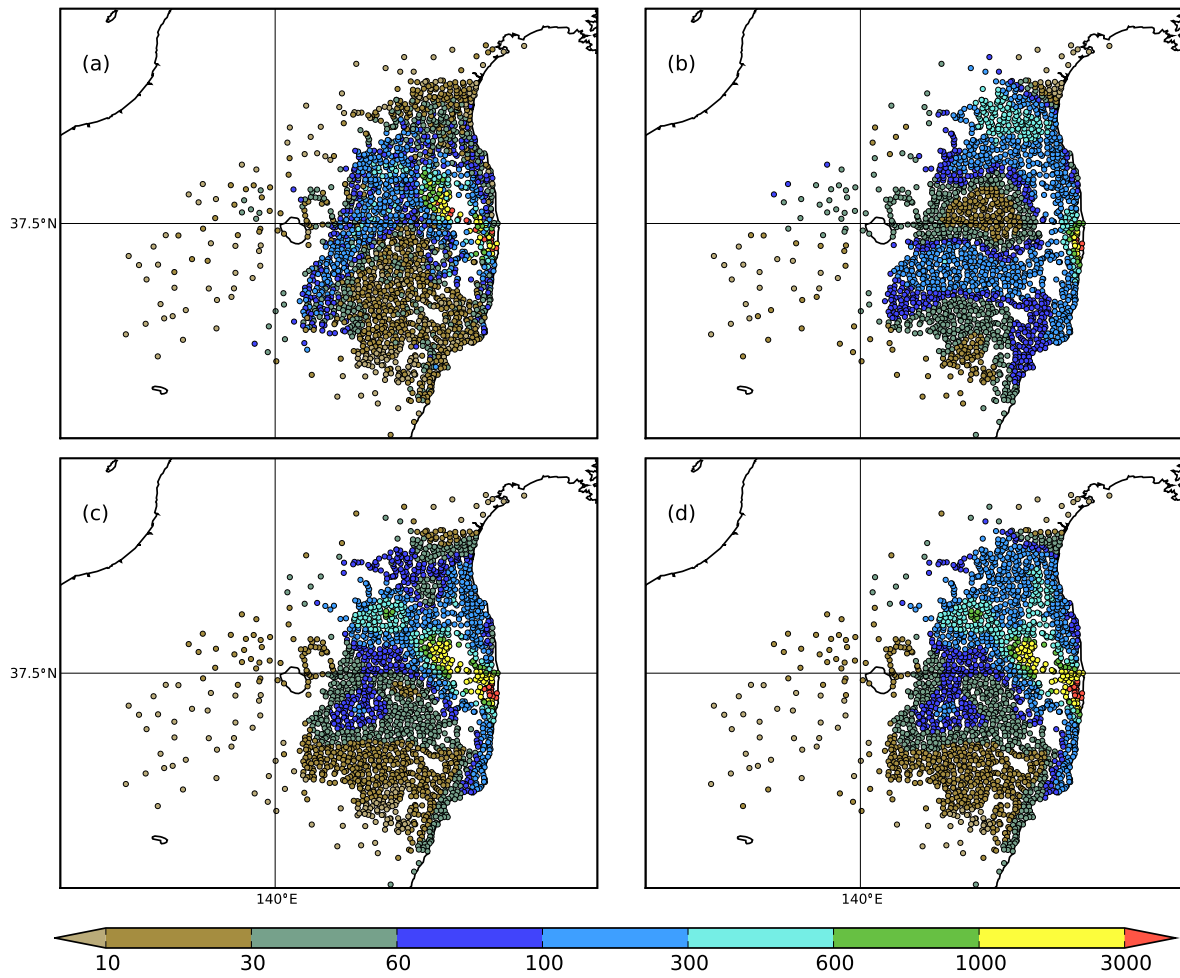


Figure 5: Map of observed and simulated deposited ^{137}Cs . Upper left (a): measurements from MEXT. Upper right (b): simulation with source reconstructed using only ^{137}Cs activity concentrations in the air. Lower left (c): simulation with source reconstructed using ^{137}Cs activity concentrations in the air, daily measurements of deposited ^{137}Cs and measurements of total cumulated deposited ^{137}Cs . Lower right (d): simulation with source reconstructed using ^{137}Cs activity concentrations in the air, daily measurements of deposited ^{137}Cs and super-observations computed from measurements of total cumulated deposited ^{137}Cs . The displayed values are in kBq m^{-2}

Table 3: Estimation of parameters and corresponding reconstructed released activity for caesium-137 source using activity concentration, fallout daily measurements and total deposition data. r_1 , r_2 and r_3 represents respectively the errors variances of these three data sets.

parameter	method	with deposition raw data	with deposition super-observations
r_1 (Bq m ⁻³)	Desroziers' scheme	3.8	2.9
	Maximum likelihood	3.3	2.3
r_2 (Bq m ⁻²)	Desroziers' scheme	580	540
	Maximum likelihood	210	240
r_3 (Bq m ⁻²)	Desroziers' scheme	325000	240000
	Maximum likelihood	320000	230000
m (Bq s ⁻¹)	Desroziers' scheme	1.2×10^{11}	1.3×10^{11}
	Maximum likelihood	1.0×10^{11}	1.0×10^{11}
Released activity (Bq)	Desroziers' scheme	1.3×10^{16}	1.9×10^{16}
	Maximum likelihood	1.2×10^{16}	1.8×10^{16}

method would consist in computing super-observations by averaging all the observations contained in a model grid cell (the model resolution is $0.05^\circ \times 0.05^\circ$), in order to mitigate the spatial correlation in the errors. This is the method that we chose. From the 2180 measurements initially in the third data set, we computed 523 super-observations from which we eliminated 4 super-observations located too close to the NPP, hence leaving 519 super-observations to be used as the new third data set. Note that it is not necessary to estimate the reduced variance of a super-observation since this is implicitly accounted for in the related hyper-parameter estimation.

3.5.1. Estimation of parameters and total released activity

The estimated hyper-parameters as well as the estimated total released activities are reported in Tab. 3. As expected, the estimated standard deviation of the error in the cumulated fallout (r_3) is significantly decreased by about 28%.

Using these data sets, the total released activity of ¹³⁷Cs is estimated to be between 1.8×10^{16} Bq and 1.9×10^{16} Bq.

3.5.2. Temporal profile and uncertainty reduction

The reconstructed source term and its uncertainty are displayed in Fig. 3(d). The uncertainty on the total released activity is estimated to be around 15% from a Monte Carlo study of 2×10^4 draws. However, it is the same absolute standard deviation, of about 3 PBq, as in the raw data sets inversion.

All the previously mentioned events are now retrieved with these data sets:

- Around 12 March: identified as the hydrogen explosion in Unit 1.

- On 13 March: identified as the ventings on Unit 3.
- On 14 and 15 March: multiple ventings and hydrogen explosions mainly concerning Unit 2 and Unit 3. The late release on 15 March is now retrieved (from 7:00 to 9:00 UTC) even if its magnitude might appear weak (see section 3.6.1 for a discussion on the magnitude of the retrieved peaks).
- On 16 March: unidentified events but which correspond to pressure drops in Unit 2 and Unit 3.
- On 18 March: unidentified events probably related to Unit 3.
- On 19 March: unidentified events which correspond to an increase in several in-situ γ -dose rate measurements. The attempts of emergency cooling with the Tokyo Fire Department means began just after these events.
- On 20 March: unidentified events concerning at least Unit 2 and Unit 3.
- From 21 March to 23 March: events corresponding to smokes emitted from Unit 2 and Unit 3.
- On 25 March: unidentified event possibly concerning Unit 2. The magnitude of this peak might appear over-estimated (see section 3.6.1 for a discussion on the magnitude of the retrieved peaks).
- On 30 March: unidentified event.

From the scatter plots of Fig. 4(b,c), it is clear that the simulated cumulated deposition data are comparable when using the source term built from raw data or from super-observations. This is also visible on the deposition maps in Fig. 5(c,d). On the other hand the system's

715 ability to simulate the two other data sets is slightly improved when using the source term retrieved from the super-observations. The assumption that the observation errors are uncorrelated led the system to give too much weight to the third raw data set in the inverse modelling algorithm. This over-confidence may be corrected when using super-observations so that the information content in the system is better balanced.

723 3.6. Discussion about the retrieved sources

724 These inversions offer an objective estimation using data assimilation techniques of what can be extracted from the data sets and the numerical model. The assimilated observations may or may not suffice to constrain the source term parameters. We showed that the cumulated deposition data alone are not sufficient to offer a satisfying chronology of the source term and that the joint assimilation of the three data sets helped to better constrain the chronology. Yet, the magnitude of the identified peaks remains questionable. The data may or may not be able to constrain them well enough, although the estimate of the total released activity seems robust.

736 3.6.1. On the magnitude of the peaks

737 It is generally thought that the main releases have occurred around March 15. These releases probably contributed the most to the north-west pattern of the deposition map. Our system, where the cumulated deposition data do not contain any information in time, may not be constrained enough by air concentration observations or daily measurements of fallout (specially before March 18) to precisely balance the contributions of the releases of March 14-15 (around 15% of the total retrieved activity), March 20 (around 13%) and March 25 (around 15%).

748 The peaks of March 20 and March 25 are not only reconstructed with the help of deposition measurements. They are both additionally explained by measurements of activity in the air from a particular monitoring station, located in Fukushima city, which measured an activity concentration of about 32 Bq.m^{-3} around March 20 and about 14 Bq.m^{-3} around March 25. It is possible that these measurements are caused by a re-suspension of previously deposited caesium-137. But resuspension is not implemented in our model, so that resuspension events are likely to be accounted for by fictitious releases in the source term. We tried and performed a new inversion using the same data as in Section 3.5 but without the measurements of this station. Indeed, the results from the super-observations showed an increase of the released activity on March 14 and 15, from 2.6 to 3.0

764 PBq (from 13% to 16% of an unchanged total emitted activity of 19 PBq), and a decrease on March 20, from 2.6 to 2.0 PBq (from 13% to 11% of the total emitted activity). Yet, no consequences were observed on the magnitude of the peak on March 25.

769 We also performed inversions using a non-null first guess inferred from independent γ -dose measurements (Saunier et al., 2013), which indicates to the system that most of the releases occurred before March 18. As a result, the total estimated released activity increased by about 15%, but the peak on March 25 still remained almost at the same level.

775 As a more drastic test and to force the system to reconstruct higher releases before March 18, we reduced the inversion window to this period. As a consequence the releases of March 15 increased (from 0.6 PBq to 2.6 PBq using the three raw data sets, and from 0.9 PBq to 3.9 PBq using the three data sets with super-observations as the third data set), but the total estimated releases decreased (respectively from 12 PBq to 5 PBq, and from 18 PBq to 11 PBq). It is consistent with the inversion using only activity concentration in the air where approximately 6 PBq were estimated to be released after this date. At the same time the reanalysis of deposition map has been degraded especially in the central area of the north-west pattern which is the most contaminated. This shows that: (i) considering only this shorter time window, the system can not properly reconstruct the deposition pattern shown in Fig. 5(a). (ii) Releases probably occurred after March 19 and may have contributed to the north-west pattern of the deposition map, but their magnitude is still difficult to estimate because of the lack of observations with a temporal information (such as activity concentration in the air) in this area. (iii) This may highlight the difficulty to model the removal processes and specially the wet deposition. It is also possible that the cumulated deposition map, whose measurements have been made several months after the accident, is not anymore faithful to the deposition events of the accident.

804 We also tested a different reconstruction resolution. Instead of reconstructing a source term with a one-hour time-step ($N = 504$), an inversion was carried out on a source term with a three-hour time-step ($N = 168$). It is generally admitted that the inversion is sensitive to the resolution of the control space (Bocquet et al., 2011) and that the system cannot generally provide reliable information at a too precise resolution (for instance the model resolution). Nevertheless, estimating the prior errors allows to compensate the impact of the control space resolution by tuning regularisation in the inversion, so that the dependence in the resolution should be

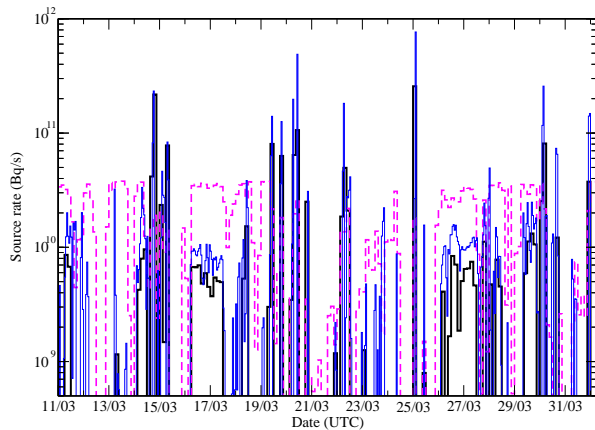


Figure 6: Full black line: Temporal profile of reconstructed caesium-137 source term with a reconstruction resolution of 3 h using the activity concentration in the air, the daily fallout measurements and the super-observations computed from the total cumulated deposited ^{137}Cs . Dashed line: posterior uncertainty of the source term computed using a Monte Carlo simulation. Thin blue line: Temporal profile of reconstructed caesium-137 source term with a reconstruction resolution of 1 h using the same data.

mitigated. The estimated source term, using the same data sets as in Section 3.5, as well as its uncertainty are displayed in Fig. 6. The total released activity is now estimated to be 1.6×10^{16} Bq with an uncertainty of 18%. The estimated released quantities were mainly reduced on March 30 (from 2.1 PBq to 1.3 PBq), on March 20 (from 2.6 PBq to 2.1 PBq) and on March 25 (from 2.9 PBq to 2.8 PBq), but remain at a high level. At the same time, the estimated released quantities increased on March 14-15 from 2.6 PBq to 4.1 PBq. Many of the low magnitude peaks with a high uncertainty have been reduced or have disappeared.

3.6.2. On the difference between the sources reconstructed with raw data and super-observations

Comparing the source profile obtained from the super-observations (Fig. 3(d)) with the source profile obtained from the inversion of the raw data sets (Fig. 3(c)), 2 PBq of caesium-137 are found to increase already existing peaks.

Moreover, when using super-observations instead of raw data, new release episodes appear in the source reconstructed term. Compared to the raw data sets inversion, 4 PBq of caesium-137 are found in new time slots. Yet the related uncertainty is still high and even above the retrieved peaks. Nonetheless, the new releases episodes that appear in the inversion do not seem to be artefacts of the inversion algorithm. They do cor-

respond to observed events in the NPP and to events reconstructed by other studies (Stohl et al., 2012; Saunier et al., 2013).

Judging from the r_i , the errors of the super-observations as well as their use by the model is diagnosed as more reliable than the use of the raw data sets. By contrast, the Tikhonov regularising term is less constraining and new peaks can more easily form in the reconstructed source term.

On a physical level, the appearance of the new peaks results from the smoothing of the deposition observations that in turn leads to a smoothing in the retrieved source. This is probably why the only peak which is reduced when using super-observations is the highest one on March 25. This peak is mainly induced by the ^{137}Cs deposit observations of the north-west very thin pattern. Hence, a smoothing of this pattern can lead to a new balance of the peaks (March 15, March 20 or March 25).

4. Conclusion

In order to reconstruct source terms of accidental pollutant releases into the atmosphere, we have proposed an inverse modelling algorithm able to use all available data in the same inversion (concentrations in the air, measurements of fallout, integrated measurements, etc.). The algorithm relies on the relationship provided by the atmospheric transport model between the source vector and the observation set and on prior errors introduced in the system: the background errors and the observation errors. To properly balance the information content in the system a proper estimation of these prior errors is crucial.

In this aim, we proposed two methods relying on the maximum likelihood principle that we applied to the challenging reconstruction of the ^{137}Cs source term released during the Fukushima Daiichi nuclear power plant accident in March 2011. Three data sets were used in the inversion process: activity concentrations in the air, daily measurements of fallout and total cumulated deposition data. Consequently, the prior estimation concerned 4 hyper-parameters: the variance of the background errors and the variance of each observation set errors. Averaged observations (called in the article super-observations) have also been considered for the third data set in order to reduce correlation in errors that had been neglected in the algorithm. Posterior uncertainty related to the estimated releases have also been estimated through a Monte Carlo analysis. Such an estimation is only possible with properly estimated prior errors.

With these methods and without super-observations, the total released activity is estimated to be between $1.2 - 1.3 \times 10^{16}$ Bq with a related uncertainty around 25%. When using super-observations instead of raw fallout data, the total released activity is estimated to be between $1.8 - 1.9 \times 10^{16}$ Bq with a related uncertainty around 15%. From our estimations the main ^{137}Cs contamination over Japan results from releases on 14-15 March, 19-20 March, 25 March and 30 March. Nevertheless, the uncertainty of each retrieved peak still remains high. Consequently the exact magnitude of the retrieved peaks has to be handled carefully. Some other significant releases might also have occurred when the wind was blowing directly towards the Pacific Ocean and are thus not totally reconstructed by our method using only data over Japan.

With the given data sets, the reconstruction of the source term could be improved on the condition that model error be better constrained. Two main influential sources of error were identified in the course of this study. Firstly, the reconstruction was found to be highly sensitive to the precipitation fields of the meteorological model. Even if the spatial distribution and chronology of the precipitation events were matching independent precipitation observations, we found it difficult to properly estimate the magnitude of those events. Secondly, with the given precipitation fields, the reconstruction remains sensitive to the physical process parameterisation in the ATM. One promising route to better constrain those processes is the inverse modelling of physical parameters (Bocquet, 2012).

Finally it seems promising to develop methods able to simultaneously reconstruct source terms of several radionuclides using all available data including γ -dose rates (Saunier et al., 2013). The number of observations, and in particular observations with an information of time, would then increase substantially. But the involved methods would certainly be more complex owing to correlations in observation errors and higher prior uncertainties in the data assimilation system.

5. Acknowledgements

This study has been supported by the IMMANENT project of Paris-Est University, and by the INSU/LEFE-ASSIM project ADOMOCA-2.

References

Abida, R., Bocquet, M., 2009. Targeting of observations for accidental atmospheric release monitoring. *Atmos. Env.* 43, 6312–6327.

Anderson, J. L., 2007. An adaptive covariance inflation error correction algorithm for ensemble filters. *Tellus A* 59, 210–224.

Bocquet, M., 2005. Reconstruction of an atmospheric tracer source using the principle of maximum entropy. I: Theory. *Q. J. R. Meteorolog. Soc.* 131, 2191–2208.

Bocquet, M., 2012. Parameter field estimation for atmospheric dispersion: Application to the Chernobyl accident using 4D-Var. *Q. J. R. Meteorolog. Soc.* 138, 664–681.

Bocquet, M., Pires, C. A., Wu, L., 2010. Beyond Gaussian statistical modeling in geophysical data assimilation. *Mon. Wea. Rev.* 138, 2997–3023.

Bocquet, M., Wu, L., Chevallier, F., 2011. Bayesian design of control space for optimal assimilation of observations. I: Consistent multiscale formalism. *Q. J. R. Meteorolog. Soc.* 137, 1340–1356.

Byrd, R. H., Lu, P., Nocedal, J., 1995. A limited memory algorithm for bound constrained optimization. *SIAM Journal on Scientific and Statistical Computing* 16, 1190–1208.

Chapnik, B., Desroziers, G., Rabier, F., Talagrand, O., 2004. Properties and first application of an error-statistics tuning method in variational assimilation. *Q. J. R. Meteorolog. Soc.* 130, 2253–2275.

Chapnik, B., Desroziers, G., Rabier, F., Talagrand, O., 2006. Diagnosis and tuning of observational error in a quasi-operational data assimilation setting. *Q. J. R. Meteorolog. Soc.* 132, 543–565.

Chino, M., Nakayama, H., Nagai, H., Terada, H., Katata, G., Yamazawa, H., 2011. Preliminary estimation of release amounts of I131 and Cs137 accidentally discharged from the Fukushima Dai-ichi nuclear power plant into the atmosphere. *Journal of Nuclear Science and Technology* 48, 1129–1134.

Davoine, X., Bocquet, M., 2007. Inverse modelling-based reconstruction of the Chernobyl source term available for long-range transport. *Atmos. Chem. Phys.* 7, 1549–1564.

Dee, D. P., 1995. On-line estimation of error covariance parameters for atmospheric data assimilation. *Mon. Wea. Rev.* 123, 1128–1145.

Delle Monache, L., Lundquist, J. K., Kosovic, B., Johannesson, G., Dyer, K. M., Aines, R. D., Chow, F. K., Belles, R. D., Hanley, W. G., Larsen, S. C., Loosmore, G. A., Nitao, J. J., Sugiyama, G. A., Vogt, P. J., 2008. Bayesian inference and Markov chain Monte Carlo sampling to reconstruct a contaminant source on a continental scale. *Journal of Applied Meteorology and Climatology* 47, 2600–2613.

Desroziers, G., Berre, L., Chapnik, B., Poli, P., 2005. Diagnosis of observation, background and analysis error statistics in observation space. *Q. J. R. Meteorolog. Soc.* 131, 3385–3396.

Desroziers, G., Ivanov, S., 2001. Diagnosis and adaptive tuning of observation-error parameters in a variational assimilation. *Q. J. R. Meteorolog. Soc.* 127, 1433–1452.

Elbern, H., Strunk, A., Schmidt, H., Talagrand, O., 2007. Emission rate and chemical state estimation by 4-dimensional variational inversion. *Atmos. Chem. Phys.* 7, 3749–3769.

Estournel, C., Bosc, E., Bocquet, M., Ulses, C., Marsaleix, P., Winiarek, V., Osvath, I., Nguyen, C., Duhaut, T., Lyard, F., Michaud, H., Auclair, F., 2012. Assessment of the amount of cesium-137 released to the Pacific Ocean after the Fukushima accident and analysis of its dispersion in the Japanese coastal waters. *J. Geophys. Res.* 117, C11014.

Hajivassiliou, V., McFadden, D., Ruud, P., 1996. Simulation of multivariate normal rectangle probabilities and their derivatives - Theoretical and computational results. *Journal of Econometrics* 72, 85–134.

Hansen, P. C., 1992. Analysis of discrete ill-posed problems by means of the L-curve. *SIAM Review* 34, 561–580.

Katata, G., Terada, H., Nagai, H., Chino, M., 2012. Numerical reconstruction of high dose rate zones due to the Fukushima Dai-ichi Nuclear Power Plant accident. *J. Environ. Radioactivity* 111, 2–12.

- 1004 Korsakissok, I., Mathieu, A., Didier, D., 2013. Atmospheric disper- 1069
1005 sion and ground deposition induced by the Fukushima Nuclear 1070
1006 Power Plant accident: A local-scale simulation and sensitivity 1071
1007 study. *Atmos. Env.* 70, 267–279. 1072
- 1008 Krysta, M., Bocquet, M., Brandt, J., 2008. Probing ETEX-II data set 1073
1009 with inverse modelling. *Atmos. Chem. Phys.* 8, 3963–3971. 1074
- 1010 Li, H., Kalnay, E., Miyoshi, T., 2009. Simultaneous estimation of 1075
1011 covariance inflation and observation errors within an ensemble 1076
1012 Kalman filter. *Q. J. R. Meteorolog. Soc.* 135, 523–533. 1077
- 1013 Liu, Z.-Q., Rabier, F., 2002. The interaction between model resolu- 1078
1014 tion, observation resolution and observation density in data assimi- 1079
1015 lation: A one-dimensional study. *Q. J. R. Meteorolog. Soc.* 128, 1080
1016 1367–1386. 1081
- 1017 Louis, J., 1979. A parametric model of vertical eddy fluxes in the 1082
1018 atmosphere. *Boundary-Layer Meteor.* 17, 197–202. 1083
- 1019 Maryon, R. H., Smith, F. B., Conway, B. J., Goddard, D. M., 1991. 1084
1020 The U.K. nuclear accident model. *Progress in Nuclear Energy* 26, 1085
1021 85–104.
- 1022 Mathieu, A., Korsakissok, I., Quélo, D., Groëll, J., Tombette, M., Di- 1086
1023 dier, D., Quentric, E., Saunier, O., Benoît, J.-P., Isnard, O., 2012. 1087
1024 Atmospheric dispersion and deposition of radionuclides from the 1088
1025 Fukushima Daiichi nuclear power plant accident. *Elements* 8, 195– 1089
1026 200.
- 1027 Ménard, R., Cohn, S. E., Chang, L.-P., Lyster, P. M., 2000. Assimila- 1090
1028 tion of stratospheric chemical tracer observations using a Kalman 1091
1029 filter. Part I: Formulation. *Mon. Wea. Rev.* 128, 2654–2671.
- 1030 Michalak, A. M., Bruhwiler, L., Tans, P. P., 2004. A geostatistical 1092
1031 approach to surface flux estimation of atmospheric trace gases. *J.* 1093
1032 *Geophys. Res.* 109, D14109.
- 1033 Mitchell, H. L., Houtekamer, P. L., 1999. An adaptive ensemble 1094
1034 Kalman filter. *Mon. Wea. Rev.* 128, 416–433.
- 1035 Quélo, D., Krysta, M., Bocquet, M., Isnard, O., Minier, Y., Sportisse, 1095
1036 B., 2007. Validation of the Polyphemus platform on the ETEX, 1096
1037 Chernobyl and Algeciras cases. *Atmos. Env.* 41, 5300–5315.
- 1038 Saide, P., Bocquet, M., Osses, A., Gallardo, L., 2011. Constraining 1097
1039 surface emissions of air pollutants using inverse modeling: method 1098
1040 intercomparison and a new two-step multiscale approach. *Tellus B* 1099
1041 63, 360–370.
- 1042 Saunier, O., Mathieu, A., Didier, D., Tombette, M., Quélo, D., 1100
1043 Winiarek, V., Bocquet, M., 2013. An inverse modeling method to 1101
1044 assess the source term of the Fukushima nuclear power plant ac- 1102
1045 cident using gamma dose rate observations. *Atmos. Chem. Phys.* 1103
1046 Discuss. 13, 15567–15614.
- 1047 Schwinger, J., Elbern, H., 2010. Chemical state estimation for the 1104
1048 middle atmosphere by four dimensional variational data assimi- 1105
1049 lation: A posteriori validation of error statistics in observation space. 1106
1050 *J. Geophys. Res.* 115, D18307.
- 1051 Skamarock, W. C., Klemp, J. B., Dudhia, J., Gill, D. O., Barker, D. M., 1107
1052 Duda, M. G., Huang, S.-Y., Wang, W., Powers, J. G., 2008. A 1108
1053 description of the advanced research WRF version 3. Tech. rep., 1109
1054 NCAR.
- 1055 Stauffer, D. R., Seaman, N. L., 1994. On multi-scale four dimensional 1110
1056 data assimilation. *J. Appl. Meteor.* 33, 416–434.
- 1057 Stohl, A., Seibert, P., Wotawa, G., Arnold, D., Burkhart, J. F., 1111
1058 Eckhardt, S., Vargas, A., Yasunari, T. J., 2012. Xenon-133 and 1112
1059 caesium-137 releases into the atmosphere from the Fukushima 1113
1060 Dai-ichi nuclear power plant: determination of the source term, 1114
1061 atmospheric dispersion, and deposition. *Atmos. Chem. Phys.* 12, 1115
1062 2313–2343.
- 1063 Terada, H., Katata, G., Chino, M., Nagai, H., 2012. Atmospheric dis- 1116
1064 charge and dispersion of radionuclides during the Fukushima Dai- 1117
1065 ichi Nuclear Power Plant accident. Part ii: verification of the source 1118
1066 term and analysis of regional-scale atmospheric dispersion. *J. En- 1119
1067 viron. Radioactivity* 112, 141–154.
- 1068 Winiarek, V., Bocquet, M., Saunier, O., Mathieu, A., 2012a. Cor- 1120
rection to "Estimation of errors in the inverse modeling of acci-
dental release of atmospheric pollutant: Application to the recon-
struction of the cesium-137 and iodine-131 source terms from the
Fukushima Daiichi power plant". *J. Geophys. Res.* 117, D18118.
- Winiarek, V., Bocquet, M., Saunier, O., Mathieu, A., 2012b. Esti-
mation of errors in the inverse modeling of accidental release of
atmospheric pollutant: Application to the reconstruction of the
cesium-137 and iodine-131 source terms from the Fukushima Dai-
ichi power plant. *J. Geophys. Res.* 117, D05122.
- Winiarek, V., Vira, J., Bocquet, M., Sofiev, M., Saunier, O., 2011.
Towards the operational estimation of a radiological plume using
data assimilation after a radiological accidental atmospheric
release. *Atmos. Env.* 45, 2944–2955.
- Yee, E., Lien, F.-S., Keats, A., D'Amours, R., 2008. Bayesian in-
version of concentration data: Source reconstruction in the adjoint
representation of atmospheric diffusion. *Journal of Wind Engineer-
ing and Industrial Aerodynamics* 96, 1805–1816.